arXiv:1610.02277v1 [cs.CE] 7 Oct 2016

Simulation of flow and view with applications in computational design of settlement layouts

Christian Valdemar Hansen[a], Anders Logg[b], Carl Lundholm[b]

[a]*Department of Mathematics and Computer Science, University of Southern Denmark, Odense.*
[b]*Department of Mathematical Sciences, Chalmers University of Technology and University of Gothenburg*

Abstract

We present methodology, algorithms and software for evaluating flow and view for architectural settlement layouts. For a given settlement layout consisting of a number of buildings arbitrarly positioned on a piece of land, in the present study an island situated on the west coast of Sweden, the methodology allows for evaluation of flow patterns and for evaluating the view experienced from the buildings. The computation of flow is based on a multimesh finite element methods, which allows each building to be embedded in a boundary-fitted mesh which can be moved around freely in a fixed background mesh. The computation of view is based on a novel and objective measure of the view which can be efficiently computed by rasterization.

Keywords: Settlement layout, computational architecture, flow, view, Stokes, multimesh, FEniCS.

1. Introduction

When designing settlement layouts, architects need to take a large number of variables into consideration, such as economic interests and connections to infrastructure (roads, water and electricity), the experienced quality of view from the buildings, wind conditions, and many more. In this study, we examine how to efficiently compute wind patterns and how to evaluate view. The aim is to provide architects with a computational tool that can be used

Email addresses: cvh@imada.sdu.dk (Christian Valdemar Hansen), logg@chalmers.se (Anders Logg), carlun@chalmers.se (Carl Lundholm)

as a guide as part of an iterative architectural design process. For a current example of a challenging design problem in architectural settlement layout, see Johansson et al. (2014). There are several examples of CFD simulations in urban environments in the literature; see, e.g., Baskaran and Kashef (1996); Blocken et al. (2007, 2011); Heuveline et al. (2011). A recent study by Ingelsten et al. (2016) investigates the simulation of flow on geometries directly defined by point clouds.

A central issue when designing a computational tool for settlement layout design is that the tool should be able to quickly evaluate a multitude of suggested designs, either as part of an optimization loop or as part of a manual (artistic) iterative design process. Standard numerical methods for computation of flow require that a computational mesh or grid is generated around both buildings, ground and other objects. Generating such a body-fitted mesh is a costly procedure and even more so when a large number of different meshes must be created, one for each configuration of the buildings.

Instead, we examine in this work the use of *multimesh* finite element methods. Multimesh finite element methods allow a problem to be posed not on a single body-fitted mesh but instead on a collection of meshes that may overlap arbitrarily and which together define the computational domain. Figure 1 gives an example of such a configuration.

By allowing the computational domain to be discretized by multiple overlapping meshes, one may freely move the overlapping meshes relative to one another, which allows a multitude of configurations to be computed and evaluated without the need for costly mesh generation. However, this flexibility comes at a price. First, one must ensure that the finite element discretization remains stable and that convergence is retained independently of the relative positions of the meshes. If the finite element method is not carefully designed and does not incorporate the correct stabilization terms, certain configurations may lead to very ill-conditioned systems, low accuracy and even blow-up. Another concern is that the formulation of multimesh finite element methods requires integration over cut cells and interfaces. This means that an implementation faces challenging problems in computational geometry, when intersections and quadrature points must be computed efficiently and robustly.

For the computation of view, we develop in this work a novel and objective measure that can be used to quantify the view for any given design. This measure may be computed efficiently using a technique from computer graphics known as *rasterization*. The measure itself allows for easy incorpo-

ration of weights that may be tweaked to give different weights to view of air, water, ground, buildings, herbage and other objects.

In the remainder of this paper, we first review in Section 2 multimesh finite element methods and their relation to existing methodologies for discretization of multiphysics problems and complex geometries. We then discuss in Sections 3 and 4 details of the algorithms and the implementation. Results are presented in Section 5 and finally we present our conclusions and discuss current limitations and future work in Section 6.

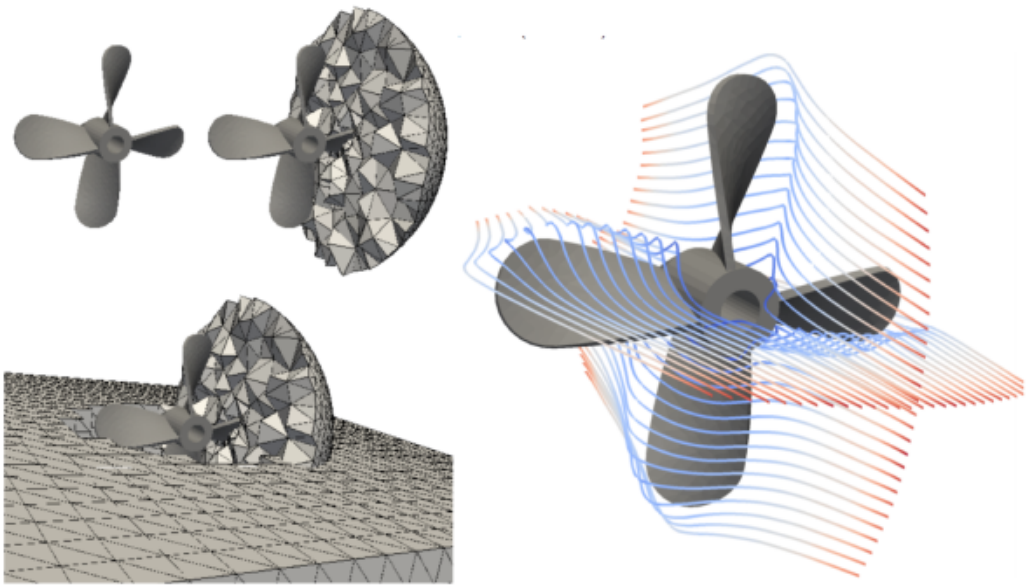

Figure 1: A collection of arbitrarily overlapping meshes together definining the computational domain, here the surroundings of a 3D propeller immersed in water. Images courtesy of Johansson et al. (2015).

2. Multimesh finite element methods

A number of methodologies have been proposed to circumvent the limitations of interface-fitted discretization. Notable examples are the fictitious domain (FD) method by Glowinski et al. (2001) and the extended finite element method (XFEM) by Belytschko et al. (Moes et al., 1999). Both methods have been successful in extending the range of problems that can be simulated, but both suffer from limitations in that the conditioning of the

discretization cannot be guaranteed, and a theoretical framework for convergence analysis and error estimation is lacking. In particular, time-dependent multiphysics problems on evolving geometries are typically discretized using *ad hoc* low order discretization methods, which cannot easily be analyzed, nor extended to higher order.

Over the past decade, a theoretical foundation for the formulation of stabilized cut FEM has been developed by extending the ideas of Nitsche (1971) to a general weak formulation of the interface conditions, thereby removing the need for interface-fitted meshes. The foundations of cut FEM were presented in Hansbo and Hansbo (2002); Hansbo et al. (2003) and the methodology has since been extended to a number of important multiphysics problems; see Burman and Fernández (2007); Burman and Hansbo (2007); Becker et al. (2009); Massing et al. (2013).

We refer to multimesh finite element methods as finite element methods based on the stabilized finite element formulations of cut FEM in combination with a flexible and general treatment of multiple and arbitrarily overlapping meshes. In addition to the theoretical foundation in cut FEM, the implementation and application of multimesh finite element methods relies on efficient and robust computation of mesh-mesh intersections in 3D. This puts high demands on the implementation and requires much more sophisticated algorithms from computational geometry than what is normally the case for finite element problems. Figure 2 illustrates a collection of body-fitted meshes that move independently through a fixed background mesh to discretize the flow around a collection of moving bodies immersed in a fluid.

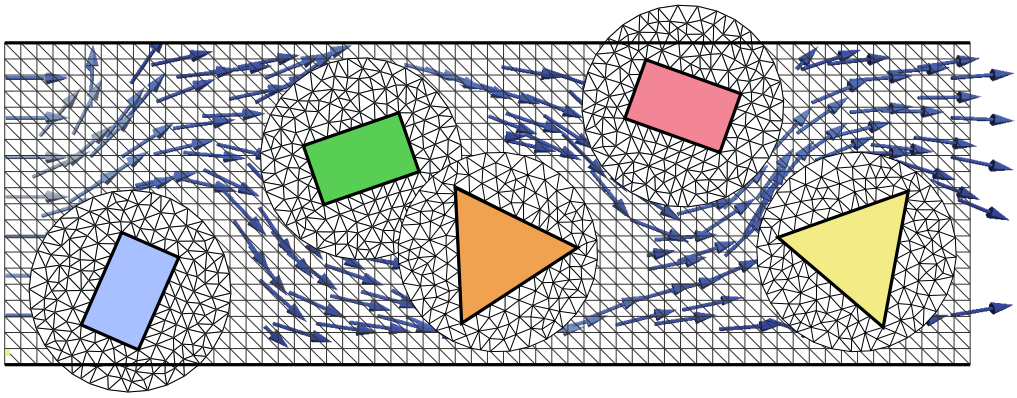

Figure 2: Multimesh discretization of the flow around a collection of bodies moving through a channel.

Support for the formulation of multimesh finite element methods has recently been added to the popular open-source finite element package FEniCS (Logg and Wells, 2010; Logg et al., 2012). With version 2016.1 of FEniCS, users may formulate and automatically discretize basic multimesh finite element formulations of systems of PDE such as the Stokes problem. The implementation in FEniCS relies on a novel implementation of mesh-mesh intersections, based on efficient generation and traversal of axis-aligned bounding box trees (AABB trees), robust low-level operations for computing and representing the intersections of triangles (2D) and tetrahedra (3D), and generation of quadrature points on cut cells. The implementation is integrated with the automatic code generation of FEniCS which allows multimesh discretizations to be formulated in (close to) natural mathematical language, as will be demonstrated in Section 4. The present study constitutes the first application of the newly implemented multimesh framework of FEniCS.

For the flow problems studied in the present work (modeled by the Stokes equations), the finite element formulation is based on the stabilized Stokes discretization analyzed by Johansson et al. (2015) as an extension to higher-order function spaces of the discretization previously analyzed by Massing et al. (2014).

3. Algorithms

We here present an overview of the methodology used to simulate the flow of air and the view for the application under consideration: the design of a settlement (placement of houses) on a small island on the west coast of Sweden.

3.1. Computation of flow

To model the flow over the island and houses, a finite element method for Stokes equations on overlapping meshes is used. The method is a slight modification of the cut finite element method for Stokes equations, presented by Johansson et al. (2015). For a bounded domain $\Omega \subset \mathbb{R}^d$ with boundary $\partial\Omega$, the strong problem formulation for Stokes equations reads: Find the velocity $\mathbf{u} : \Omega \to \mathbb{R}^d$ and the pressure $p : \Omega \to \mathbb{R}$ such that

$$\begin{cases} -\Delta \mathbf{u} + \nabla p = \mathbf{f} & \text{in } \Omega, \\ \nabla \cdot \mathbf{u} = 0 & \text{in } \Omega, \\ \mathbf{u} = \mathbf{0} & \text{on } \partial\Omega, \end{cases} \tag{1}$$

where $\mathbf{f} : \Omega \to \mathbb{R}^d$ is a given right-hand side. To obtain a finite element formulation for Stokes equations on two overlapping meshes, we start by considering two separate bounded domains $\widehat{\Omega}_0$ and $\widehat{\Omega}_1$, called predomains. We may place $\widehat{\Omega}_1$ on top of $\widehat{\Omega}_0$. Let $\Omega_0 := \widehat{\Omega}_0 \setminus \widehat{\Omega}_1$ and $\Omega_1 := \widehat{\Omega}_1$, with boundaries $\partial\Omega_0$ and $\partial\Omega_1$, respectively. We define the solution domain by $\Omega := \Omega_0 \cup \Omega_1$ and the joint boundary between Ω_0 and Ω_1 by $\Gamma := \partial\Omega_0 \cap \partial\Omega_1$. Proceeding in the usual way, by introducing suitable function spaces, multiplying the equations with test functions, and integrating by parts, one arrives at the variational formulation of the problem. To get the corresponding finite element formulation, the predomains, $\widehat{\Omega}_0$ and $\widehat{\Omega}_1$, are tessellated to create the meshes $\widehat{\mathcal{K}}_{h,0}$ and $\widehat{\mathcal{K}}_{h,1}$, respectively. We call $\widehat{\mathcal{K}}_{h,0}$ the background mesh, and $\widehat{\mathcal{K}}_{h,1}$ the overlapping mesh. This gives us a mesh hierarchy on which we define a finite element space for the velocity, $\mathbf{V}_h$, and a finite element space for the pressure, Q_h. Here, Taylor-Hood elements are used to ensurethe stability of the solution, i.e., polynomials of degree two for the velocity and polynomials of degree one for the pressure. The finite element formulation for Stokes equations on two overlapping meshes reads: Find $(\mathbf{u}_h, p_h) \in \mathbf{V}_h \times Q_h$ such that

$$
\begin{aligned}
& (D\mathbf{u}_h, D\mathbf{v})_{\Omega_0} + (D\mathbf{u}_h, D\mathbf{v})_{\Omega_1} \\
& - (\langle (D\mathbf{u}_h)\cdot\mathbf{n}\rangle, [\mathbf{v}])_\Gamma - ([\mathbf{u}_h], \langle (D\mathbf{v})\cdot\mathbf{n}\rangle)_\Gamma \\
& + \beta h^{-1}([\mathbf{u}_h], [\mathbf{v}])_\Gamma + ([D\mathbf{u}_h], [D\mathbf{v}])_{\Omega_{h,0}\cap\Omega_1} \\
& - (\nabla\cdot\mathbf{u}_h, q)_{\Omega_0} - (\nabla\cdot\mathbf{u}_h, q)_{\Omega_1} + ([\mathbf{n}\cdot\mathbf{u}_h], \langle q\rangle)_\Gamma \\
& - (\nabla\cdot\mathbf{v}, p_h)_{\Omega_0} - (\nabla\cdot\mathbf{v}, p_h)_{\Omega_1} + ([\mathbf{n}\cdot\mathbf{v}], \langle p_h\rangle)_\Gamma \\
& + \gamma([p_h], [q])_{\Omega_{h,0}\cap\Omega_1} + h^2(\Delta\mathbf{u}_h - \nabla p_h, \Delta\mathbf{v} + \nabla q)_{\Omega_{h,0}\setminus\omega_{h,0}} \\
= \quad & (\mathbf{f}, \mathbf{v})_{\Omega_0} + (\mathbf{f}, \mathbf{v})_{\Omega_1} - h^2(\mathbf{f}, \Delta\mathbf{v} + \nabla q)_{\Omega_{h,0}\setminus\omega_{h,0}},
\end{aligned}
\tag{2}
$$

for all $(\mathbf{v}, q) \in \mathbf{V}_h \times Q_h$. Here, $\mathbf{n}$ is the unit normal to Γ exterior to Ω_1, $\langle v\rangle = (v_0 + v_1)/2$ is the average of v on Γ (v_i is the limit of v on Ω_i as we approach Γ, for $i = 0, 1$), $[v] = v_1 - v_0$ is the jump in v on Γ, $\Omega_{h,0} \cap \Omega_1$ is the *overlapped* part of all the background cells that are cut by Γ, $\Omega_{h,0} \setminus \omega_{h,0}$ is the *visible* part of all the background cells that are cut by Γ, h is the mesh size, and β and γ are stability parameters. For more details on the method, see Johansson et al. (2015).

The stability term $\gamma([p_h], [q])_{\Omega_{h,0}\cap\Omega_1}$ has been added to the original formulation of the method presented in Johansson et al. (2015), and is the

slight modification mentioned earlier. Numerical tests have indicated that the presence of this stability term increases the robustness of the method, in particular for the pressure. This indicates that further analysis of the original formulation may be of interest.

For the application studied in this work, the background mesh is also referred to as the air mesh, since it discretizes the air above the island. The overlapping meshes are also referred to as house meshes, since they contain the houses. We are now ready to formulate the algorithm for obtaining the flow over the island and houses by solving (2).

Algorithm 1 Flow model

1: Geometries for the island and houses are imported. See Figure 3.
2: Meshes are generated around the geometries. For the house meshes, cells are also generated *inside* the houses. See Figures 4 and 5.
3: The house meshes are placed inside the air mesh. See Figures 6- 8.
4: Boundary conditions (inlet, outlet and no-slip) are set on the air mesh.
5: A no-slip boundary condition is applied to all facets belonging to house mesh cells that are not entirely inside the air mesh and also to facets belonging to house mesh cells that are inside the house. For more details see Figure 9.
6: The linear system of equations, resulting from (2), is solved.

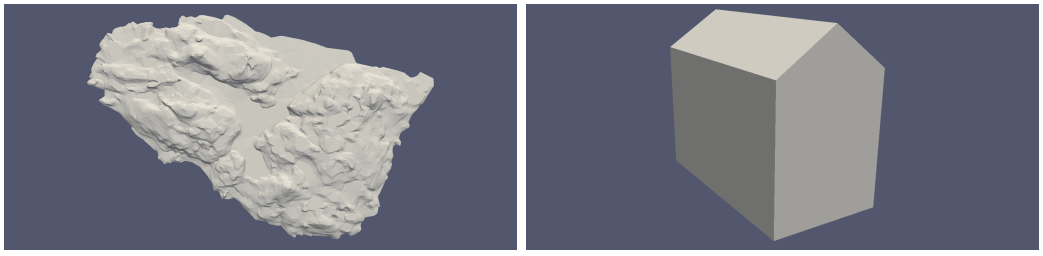

Figure 3: *Left*: Geometry of the island. *Right*: Geometry of a simplified house.

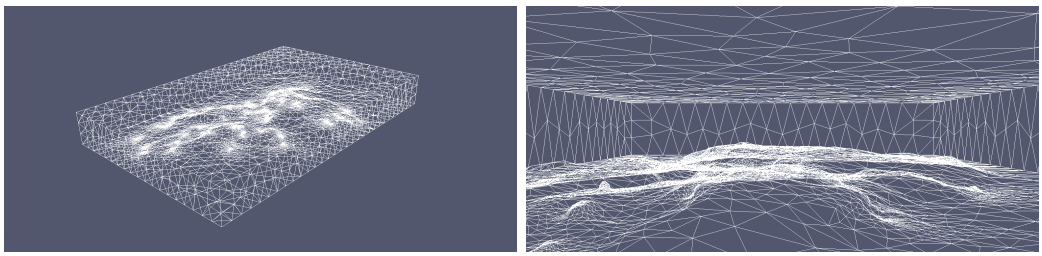

Figure 4: Air mesh viewed from the outside and from the inside.

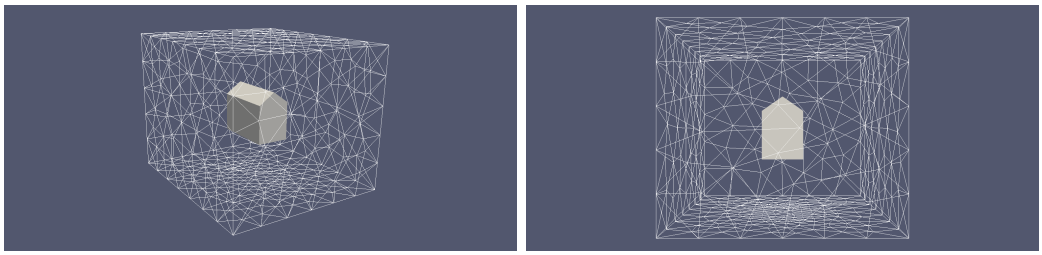

Figure 5: House mesh viewed from two different angles.

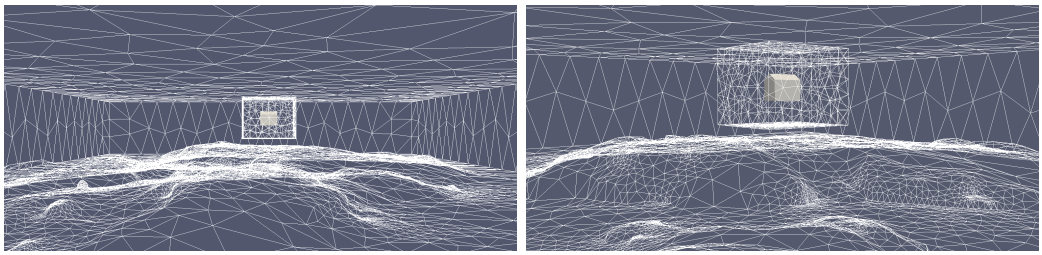

Figure 6: House mesh inside air mesh viewed from two different angles.

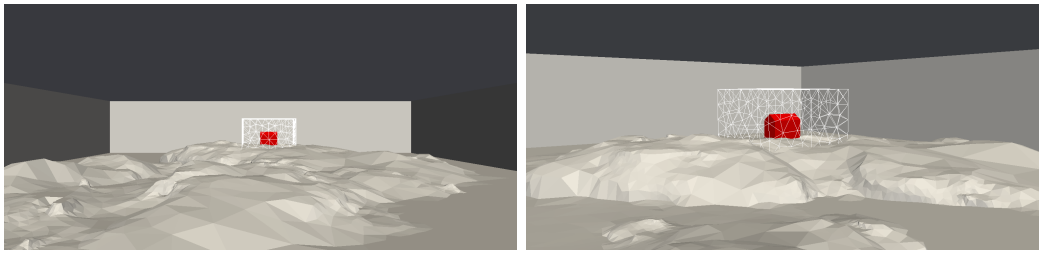

Figure 7: House mesh placed on the surface of the island viewed from two different angles.

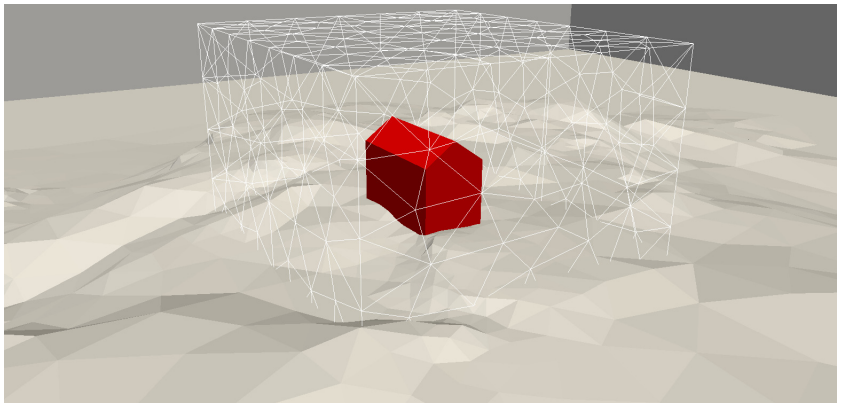

Figure 8: Closeup on the placed house mesh.

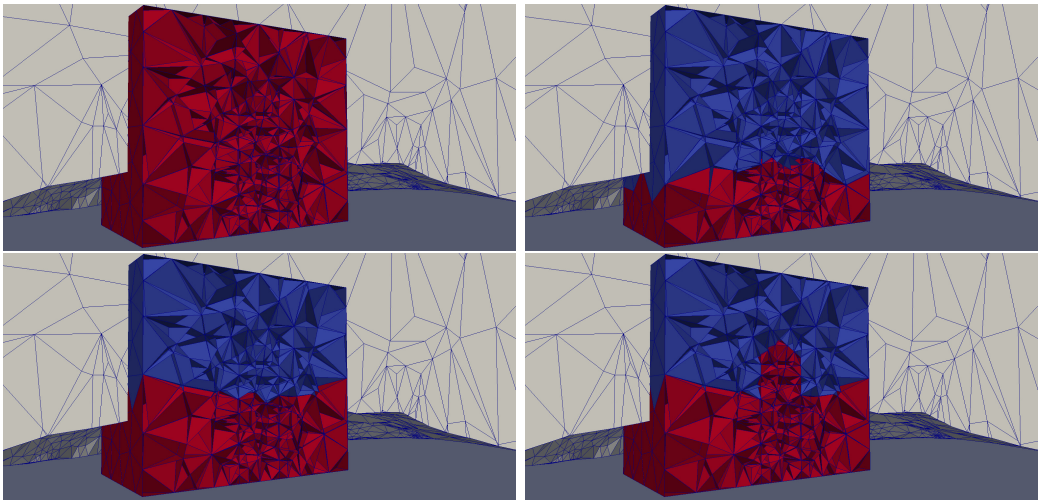

Figure 9: Cross sections of a house mesh with a cross section of the air mesh added for reference. Red facets are marked for no-slip, blue facets are not. *Top left*: Initially all facets are marked for no-slip. *Top right*: First facets intersected by the air mesh are removed. *Bottom left*: Then facets cut by the boundary of the air mesh are added. *Bottom right*: Finally facets of the house are added.

3.2. Computation of view

We here present a novel and objective measure for evaluating the view from a location such as the window of a building. The measure assigns a value V between zero and one, zero being the worst possible view and one the best possible view.

It is interesting to first consider the best and the worst cases. In the present case, the worst case would occur if the view is nothing else than another house; see illustration in Figure 10. Thus in this case the view should evaluate to $V = 0$. The best case $V = 1$ is a view consiting entirely of sea and sky; see Figure 11.

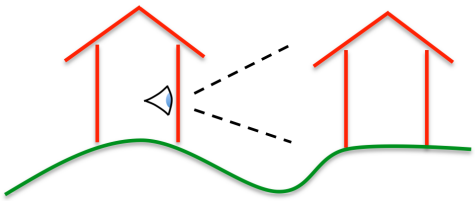

Figure 10: Worst case: $V \approx 0$.

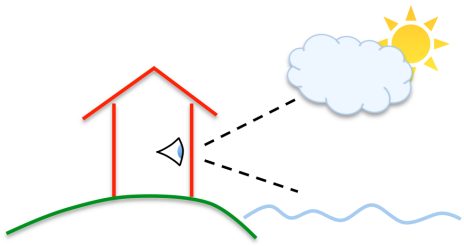

Figure 11: Best case: $V = 1$.

Examining again the worst case, the distance to a neighbouring house should influence the value of the view. In general, the negative impact of objects on the view should decrease by the distance. Our proposed measure of view is expressed as an integral over the integration domain $\omega = \omega_\phi \times \omega_\theta$ of size $|\omega|$:

$$V = \frac{1}{|\omega|} \iint_{\omega} \sigma(\phi, \theta) \, \mathrm{d}\phi \, \mathrm{d}\theta \ . \tag{3}$$

Here, $\sigma(\phi, \theta)$ is the weight of the object viewed at the angle (ϕ, θ). This weight must take a value between zero and one. In the present study, we have used the following weights:

$$\sigma(\phi, \theta) = \begin{cases} 1, & \text{if water,} \\ 1, & \text{if sky,} \\ 2 \cdot s\left(w(\phi, \theta) \frac{l(\phi, \theta)}{L}\right) - 1, & \text{otherwise,} \end{cases} \tag{4}$$

where $s(t)$ is the Sigmoid function

$$s(t) = \frac{1}{1 + e^{-t}}, \tag{5}$$

and $l(\phi, \theta)$ is the distance to the nearest object viewed at the angle (ϕ, θ). The specific element weight $w(\phi, \theta)$ is set to be 0.1 and 0.7 if there is a house

or ground viewed at (ϕ, θ), respectively. Based on the premise that $\sigma(\phi, \theta) = 0.9$ for a house viewed at (ϕ, θ) and placed at the horizon approximately 5 kilometers away, the constant L is found to be 0.17 km.

Equation (3) weights the view independent of the cardinal direction. However, in northern countries like Sweden, a southern view is often weighted higher than northern view because of the sunlight. Thus, to obtain a view formula which can depend on the cardinial direction, we let $\theta \in [0, 2\pi]$ be the angle in the horizontal plane. Let south be at $\theta = 0$, consequently $\theta = \pi$ is the northern direction. Assuming that one would weight the view in the south direction three times as high as the view in the north direction, the cardinal direction weight function could be expressed by

$$D(\theta) = 1 + \frac{1}{2}\sin(\theta - 3\pi/2) \ . \tag{6}$$

For a 360° horizontal view valuation, we now introduce $D(\theta)$ in (3). We may thus make the following modification to the measure of view:

$$V_{360} = \frac{1}{|\omega|}\int_0^{2\pi} D(\theta) \int_{\omega_\phi} \sigma(\phi, \theta)\, \mathrm{d}\phi\, \mathrm{d}\theta \ . \tag{7}$$

Note that $V_{360} \in [0, 1]$.

4. Implementation

4.1. Implementation of flow computation

The flow model has been implemented with the open-source finite element software FEniCS. Simulations of the flow model have been run with FEniCS v2016.1 on a MacBook Pro with operating system OS X Yosemite version 10.10.5, a 3.1 GHz Intel Core i7 processor and 16 GB RAM.

The island geometry has been imported as an STL-file and placed on the bottom of a sufficiently large box. The air mesh has then been generated and stored as an XML-file by the use of functionality provided by the FEniCS-package mshr. The geometries for the simplified houses have been made in Gmsh (Geuzaine and Remacle, 2009). The house meshes have also been generated with Gmsh and then converted to XML-files. To demonstrate how the FEniCS multimesh functionality is used to implement the flow model, we present the following code-snippets.

Python code

```
from dolfin import *

# Read the meshes from file
mesh_air = Mesh("mesh_air.xml")
mesh_house1 = Mesh("mesh_house1.xml")
mesh_house2 = Mesh("mesh_house2.xml")

# Initialize multimesh, add meshes and build
multimesh = Multimesh()
multimesh.add(mesh_air)
multimesh.add(mesh_house1)
multimesh.add(mesh_house2)
multimesh.build()
```

The order in which the meshes are added will create a mesh hierarchy, where the latest added mesh will be on the top. A multimesh may then be used to create finite element function spaces that are used to define the trial and test functions.

Python code

```
# Create function space
P2 = VectorElement("P", tetrahedron, 2)
P1 = FiniteElement("P", tetrahedron, 1)
TH = P2 * P1
W  = MultiMeshFunctionSpace(multimesh, TH)

# Define trial and test functions
(u, p) = TrialFunctions(W)
(v, q) = TestFunctions(W)
```

Here, Taylor-Hood elements of degree 2/1 are created. The trial and test functions are used to define the bilinear and linear forms, which are in turn are used to assemble the system matrix and load vector, respectively, for the linear system of equations.

Python code

```
# Define facet normal, mesh size and stability parameters
n = FacetNormal(multimesh)
h = 2.0*Circumradius(multimesh)
beta = Constant(1e1)
gamma = Constant(1e8)

def tensor_jump(v, n):
    return outer(v('+'), n('+')) + outer(v('-'), n('-'))
```

```
def a_h(v, w):
    return inner(grad(v), grad(w))*dX \
         - inner(avg(grad(v)), tensor_jump(w, n))*dI \
         - inner(avg(grad(w)), tensor_jump(v, n))*dI \
         + beta/avg(h) * inner(jump(v), jump(w))*dI

def b_h(v, q):
    return -div(v)*q*dX + jump(v, n)*avg(q)*dI

def l_h(v, q, f):
    return inner(f, v)*dX

def s_O(v, w):
    return inner(jump(grad(v)), jump(grad(w)))*dO

def s_C(v, q, w, r):
    return h*h*inner(-div(grad(v)) + grad(q),
                     -div(grad(w)) - grad(r))*dC

def l_C(v, q, f):
    return h*h*inner(f, -div(grad(v)) - grad(q))*dC

def s_P(q, r):
    return gamma * inner(jump(q), jump(r))*dO

# Define bilinear form
a = a_h(u, v) + b_h(v, p) + b_h(u, q) + s_O(u, v) \
    + s_C(u, p, v, q) + s_P(p, q)

# Define linear form
L  = l_h(v, q, f) + l_C(v, q, f)

# Assemble linear system
A = assemble_multimesh(a)
b = assemble_multimesh(L)
```

Note the resemblence of the code to the mathematical notation used in the finite element formulation (2). Then boundary conditions for the air mesh are created and applied to the system matrix and load vector.

Python code

```
# Mark boundaries for air mesh
facet_markers_air = FacetFunction("size_t", mesh_air)
facet_markers_air.set_all(0)
```

```
noslip_boundary.mark(facet_markers_air, 1)
inflow_boundary.mark(facet_markers_air, 2)
outflow_boundary.mark(facet_markers_air, 3)

# Create boundary conditions
bc0 = MultiMeshDirichletBC(V, noslip_value,
                           facet_markers_air, 1, 0)
bc1 = MultiMeshDirichletBC(V, inflow_value,
                           facet_markers_air, 2, 0)
bc2 = MultiMeshDirichletBC(Q, outflow_value,
                              facet_markers_air, 3, 0)

# Apply boundary conditions
bc0.apply(A, b)
bc1.apply(A, b)
bc2.apply(A, b)
```

The no-slip condition for the concerned facets of the house meshes are created and applied in a similar fashion. Finally, the linear system is solved and the solution components on the different meshes are extracted.

Python code

```
# Compute solution
w = MultiMeshFunction(W)
solve(A, w.vector(), b)

# Extract solution components
u_air = w.part(0).sub(0)
p_air = w.part(0).sub(1)
u_house1 = w.part(1).sub(0)
p_house1 = w.part(1).sub(1)
u_house2 = w.part(2).sub(0)
p_house2 = w.part(2).sub(1)
```

4.2. Implementation of view computation

Given the mesh constructed for the flow simulation, it is now possible to visualize the view from a given point. In practice we do this by rendering an image from the 3D mesh with the use of the rasterization rendering technique. This technique goes back to Catmull (1974); Pineda (1988); Heckbert (1989). The rasterization algorithm projects the triangles from the 3D mesh onto a 2D image.

The projecting principle is sketched in Figure 12, where the vertices which are mapped onto the 2D image plane are used to check which pixels the

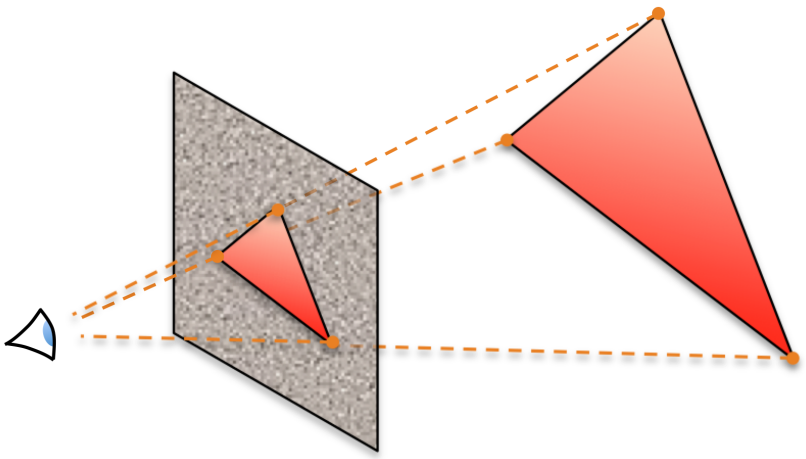

Figure 12: Projection of triangles from the 3D mesh onto the 2D image.

triangle covers. The naive idea is to loop across all the pixels in the image and check if they are inside the projected triangle or not. The efficiency of this approach depends on the size of the triangles. To account for small triangles, one may optimize the search by only searching the pixels which lie inside the bounding box of the triangle. In Figure 13, the blue square around the triangle illustrates the bounding box for which the corner coordinates are rounded to the nearest pixel.

This can be optimized further by not checking all the pixels inside the bounding box, but starting in the pixel which contains the top-point of the triangle. Then go stepwise down and check the pixels to the left and right of the reference point. If we already visited one or more pixels which are inside the projected triangle and then come to a pixel which is not in the triangle, the search stops in that direction. The search algorithm is illustrated with the green lines in Figure 13. There are several ways to optimize this, see Pineda (1988) for further reading.

Looping over all the triangles to do the projections one by one, can cause two or more projected triangles to overlap. To decide which one that should be shown in the image we have to look at the distance to the them. The distances to the triangles which are already shown in the image are stored in a two dimensional array with the same dimension as the image. Thus only the element with the shortest distance is shown in the image.

The rasterization algorithm is implemented in C++ and by the use of the

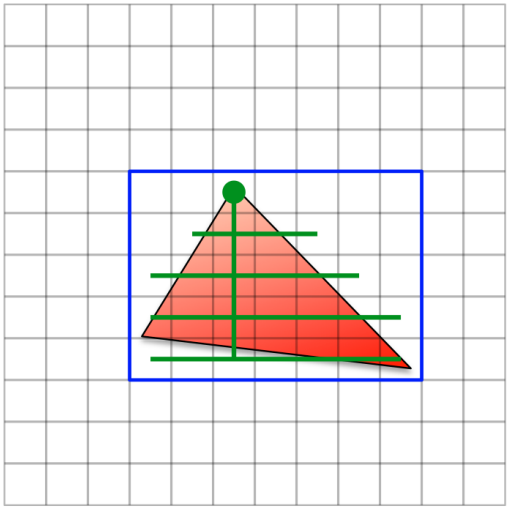

Figure 13: To check which pixels that lies inside the triangle, we start from the top-point of the triangle (the green dot) going down one step at a time to check if the pixels to the left and right are contained in the triangle.

SWIG interface compiler it is possible to access the rasterization algorithm from the C++ code in a Python script. The rasterization algorithm needs as input a list of FEniCS (.xml) meshes, where the first mesh in the list should be the main island mesh, and the rest house meshes. With the scene set, the algorithm needs to know the size of the image, both the size in pixels and the real size measured in the same units as the meshes. Also the position of the camera and the distance between the camera and the image is needed. The direction for the camera expressed by a vector should also be given. With these inputs, the algorithm generates the image and a matrix $\mathbf{S}$ which has the same size as the image and contains a value for σ for each pixel. The view valuation V is then found from $\mathbf{S}$ and given as output.

The view V may thus be computed from the image of the view generated by rasterization. If we want to compute the 360° view from (7), the domain ω is assumed to be either a cylinder or a sphere. As the rasterization algorithm generates flattened images, (7) cannot be used directly. However (7) could be estimated by

$$V_{360} = \sum_{i=0}^{N-1} \frac{D\left(2\pi i/N\right)}{N} V_i \ , \tag{8}$$

where $N \geq 3$ is the number of images and V_i is the view valuation for image

number i. It is important that no images are overlapping and that they, when joined together, form the boundary of a convex polygon with N edges, when seen from above. Thus V_i is evaluated in the direction with angle $2\pi i/N$ with respect to south and an image width of $2d\tan(\pi/N)$, where d is the distance between the camera and the image.

5. Results

5.1. Flow

Results from two simulations using the multimesh finite element method for Stokes equations on overlapping meshes (2) are presented. The first simulation was run with one overlapping house mesh and the results can be seen in Figures 14 and 15. The other simulation was run with two overlapping house meshes and the results can be seen in Figures 16 and 18. The results are in the form of tubed streamlines from the velocity field of the finite element solution. Tubes from the solution on the house mesh are made thicker than the ones from the air mesh for illustration purposes. The flow in all the figures goes from left to right.

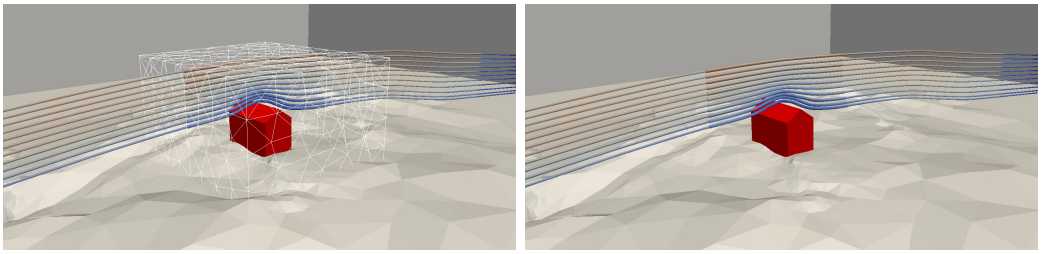

Figure 14: Tubed streamlines from the simulation with *one* overlapping house mesh. With and without the house mesh visible. Notice the continuous velocity field going between the two different meshes used for discretization.

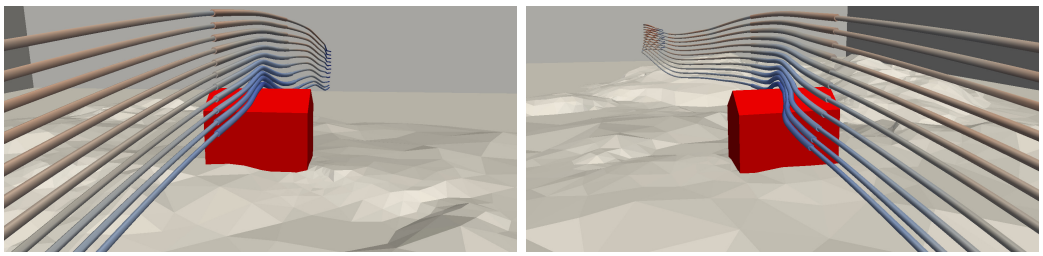

Figure 15: Tubed streamlines from the simulation with *one* overlapping house mesh. In front of and behind the house.

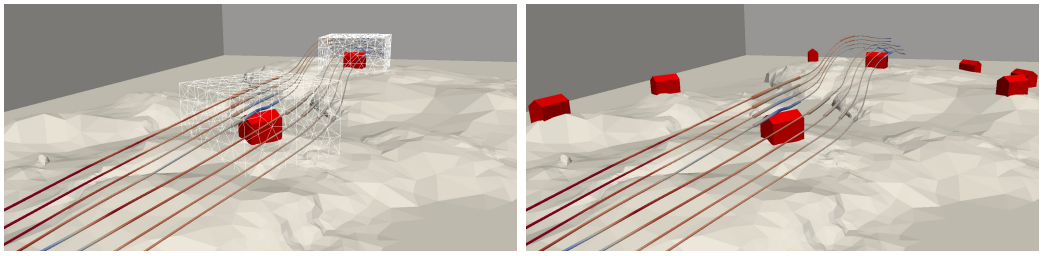

Figure 16: Tubed streamlines from the simulation with *two* overlapping house meshes. *Left*: Overview with the house meshes visible. *Right*: Overview without the house meshes visible but with some extra houses added for illustration.

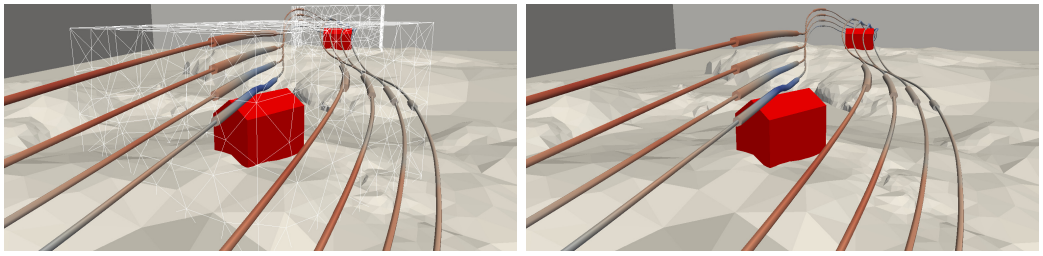

Figure 17: Tubed streamlines from the simulation with *two* overlapping house meshes. Closeup on the first house with and without the house meshes visible.

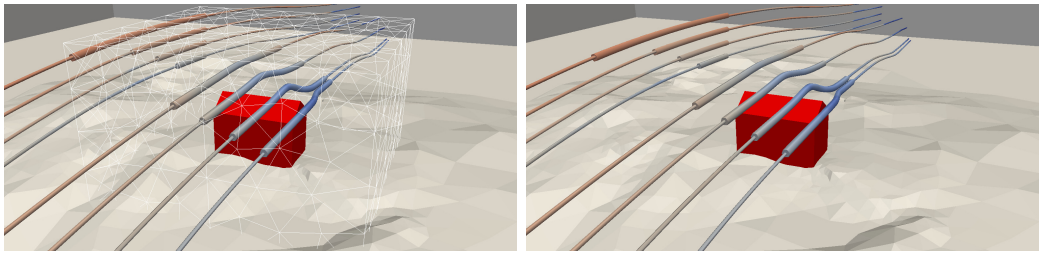

Figure 18: Tubed streamlines from the simulation with *two* overlapping house meshes. Closeup on the second house with and without the house mesh visible.

5.2. View

To test the computation of view, houses were arbitrarily positioned on the island as seen in Figure 19.

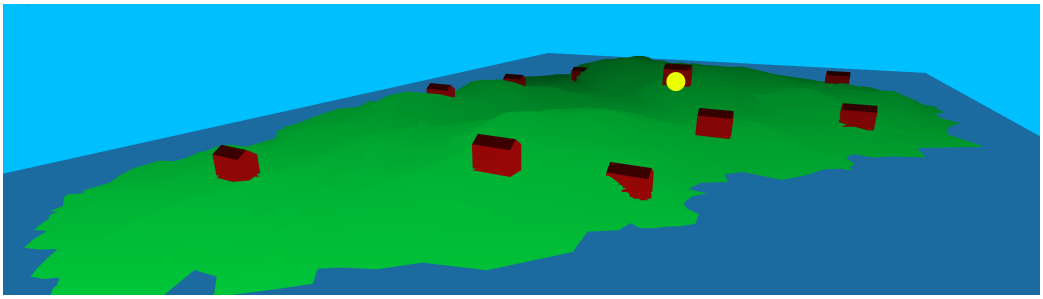

Figure 19: Overview of the island with ten houses. The yellow dot represents the position of the camera for the view computation.

For this test case we would like to examine how attractive it is to place a new house at the yellow dot, just next to the already existing house. The views in Figures 20–23 are all views from the camera located at the yellow dot in Figure 19.

Figures 20–23 show a variety of views from the selected location. Figure 20 shows a fair view with a lot of sky and sea view but also three houses and a part of the island can be seen. Therefore the view valuation becomes $V = 0.74$. To get a better view there should be as much sea or sky as possible and less houses and ground. A better example can be seen in Figure 21, where $V = 0.87$. Examples of views from the other end of the view scale can be found in Figure 22 and 23, where a neighbouring house blocks the view. In Figure 23 one can almost only see the neighbouring house, which also results in a very low value of the view.

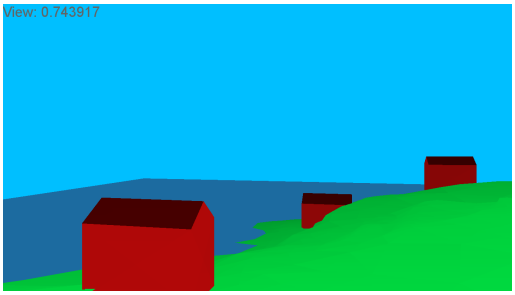

Figure 20: Fair view: $V = 0.74$

Figure 21: Good view: $V = 0.87$

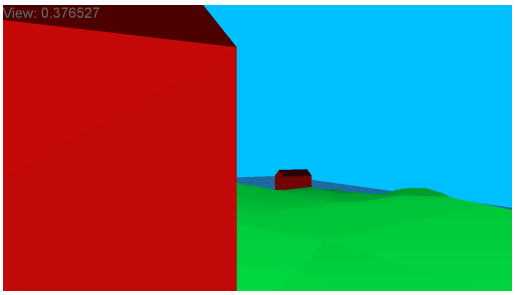

Figure 22: Poor view: $V = 0.38$

Figure 23: Bad view: $V = 0.02$

The 360° horizontal view measure (8) naturally depends on the cardinal direction. We compute the value based on 32 computed rasterizations. If the south direction is chosen to be in the direction of the view, we obtain the value $V_{360} = 0.68$ (as a result of looking straight at a neighboring house), whereas if we choose the south direction to be in the opposite direction of the neighbouring house we obtain $V_{360} = 0.73$.

6. Conclusions and future work

We have presented a generic framework for evaluating flow and view for settlement layouts. The framework allows multiple configurations to be computed and evaluated with relative ease. The current proof-of-concept implementation has several limitations that will be addressed in future work. These limitations and extensions fall into three different categories: efficiency, robustness and ease of use.

Regarding efficiency, the current implementation of multimesh methods adds a significant overhead in computational time compared to standard fi-

nite element methods. In particular, the assembly of multimesh finite element variational forms is significantly slower than standard assembly. Another limitation is the lack of a properly preconditioned iterative method (the current implementation uses the direct sparse solver UMFPACK). Both these limitations are the focus of ongoing work. Future work will also consider the extension of the current multimesh implementation to parallel architectures.

Regarding robustness, we noticed during this study that some particular configurations of buildings resulted in numerical instabilities. This is likely due to bugs or untreated corner cases in the computational geometric framework of the FEniCS multimesh implementation. This issue is also the focus of ongoing work.

To be a useful tool in an iterative architectural process, the framework must not only be efficient and robust. It must also be easy to use. Future work will also consider the creation of a user-friendly interface. In particular, it would be highly relevant to consider the creation of VR or AR interfaces to our framework.

Acknowledgements

This work was supported by the profile area *Virtual Cities* as part of *Building Futures*, an Area of Advance at Chalmers. We are also greatful towards CREAM Architects in Gothenburg for ideas, feedback and inspiration during this project.

References

References

Baskaran, A., Kashef, A., 1996. Investigation of air flow around buildings using computational fluid dynamics techniques. Engineering Structures 18 (11), 861–875.

Becker, R., Burman, E., Hansbo, P., 2009. A Nitsche extended finite element method for incompressible elasticity with discontinuous modulus of elasticity. Comp. Methods Appl. Mech. Engrg. 198 (41), 3352–3360.

Blocken, B., Carmeliet, J., Stathopoulos, T., 2007. Cfd evaluation of wind speed conditions in passages between parallel buildings—effect of wall-function roughness modifications for the atmospheric boundary layer flow. Journal of Wind Engineering and Industrial Aerodynamics 95 (9), 941–962.

Blocken, B., Stathopoulos, T., Carmeliet, J., Hensen, J. L., 2011. Application of computational fluid dynamics in building performance simulation for the outdoor environment: an overview. Journal of Building Performance Simulation 4 (2), 157–184.

Burman, E., Fernández, M. A., 2007. Stabilized explicit coupling for fluid-structure interaction using Nitsche's method. C. R. Math. Acad. Sci. Paris 345 (8), 467–472.

Burman, E., Hansbo, P., 2007. A unified stabilized method for Stokes' and Darcy's equations. J. Comput. Appl. Math. 198 (1), 35–51.

Catmull, E. E., 1974. A subdivision algorithm for computer display of curved surfaces. Ph.D. thesis, The University of Utah.

Geuzaine, C., Remacle, J.-F., 2009. Gmsh: A 3-d finite element mesh generator with built-in pre-and post-processing facilities. International Journal for Numerical Methods in Engineering 79 (11), 1309–1331.

Glowinski, R., Pan, T. W., Hesla, T. I., Joseph, D. D., Periaux, J., 2001. A fictitious domain approach to the direct numerical simulation of incompressible viscous flow past moving rigid bodies: application to particulate flow. J. Comput. Phys. 169 (2), 363–426.

Hansbo, A., Hansbo, P., 2002. An unfitted finite element method, based on Nitsche's method, for elliptic interface problems. Comp. Methods Appl. Mech. Engrg. 191 (47), 5537–5552.

Hansbo, A., Hansbo, P., Larson, M. G., 2003. A finite element method on composite grids based on Nitsche's method. ESAIM, Math. Model. Numer. Anal. 37 (03), 495–514.

Heckbert, P. S., 1989. Fundamentals of texture mapping and image warping. Tech. rep., University of California at Berkeley, Berkeley, CA, USA.

Heuveline, V., Ritterbusch, S., Ronnas, S., 2011. Augmented reality for urban simulation visualization. Preprint Series of the Engineering Mathematics and Computing Lab 0 (16).

Ingelsten, S., Mark, A., Edelvik, F., Logg, A., Österbring, M., 2016. Urban cfd-simulation using point cloud data. In: Proceedings of NSCM-26: the 26th Nordic Seminar on Computational Mechanics.

Johansson, A., Larson, M. G., Logg, A., 2015. High order cut finite element methods for the Stokes problem. Advanced Modeling and Simulation in Engineering Sciences 2 (1), 1–23.
URL http://dx.doi.org/10.1186/s40323-015-0043-7

Johansson, G., Karlén, F., Stark, M., 2014. Lilla fjellsholmen, varsamt byggande i en unik skärgårdsmiljö. Master's thesis, Chalmers University of Technology, Gothenburg, Sweden.

Logg, A., Mardal, K.-A., Wells, G. N., et al., 2012. Automated Solution of Differential Equations by the Finite Element Method. Springer.

Logg, A., Wells, G. N., 2010. DOLFIN: Automated finite element computing. ACM Transactions on Mathematical Software 37 (2).
URL http://www.dspace.cam.ac.uk/handle/1810/221918/

Massing, A., Larson, M. G., Logg, A., Rognes, M. E., 2013. An overlapping mesh finite element method for a fluid-structure interaction problem. submitted to Communications in Applied Mathematics and Computational Science.

Massing, A., Larson, M. G., Logg, A., Rognes, M. E., 2014. A stabilized nitsche overlapping mesh method for the stokes problem. Numerische Mathematik, 1–29.

Moes, N., Dolbow, J., Belytschko, T., 1999. A finite element method for crack growth without remeshing. Int. J. Numer. Meth. Engng 46, 131–150.
URL http://venus.usc.edu/PAPERS/MultiScaleMechanics/XFEM.pdf

Nitsche, J., 1971. Über ein Variationsprinzip zur Lösung von Dirichlet-Problemen bei Verwendung von Teilräumen, die keinen Randbedingungen unterworfen sind. In: Abhandlungen aus dem Mathematischen Seminar der Universität Hamburg. Vol. 36. Springer, pp. 9–15.

Pineda, J., 1988. A parallel algorithm for polygon rasterization. In: In Proceedings of Siggraph '88. pp. 17–20.